Long-term stable electroosmotic pump with ion exchange membranes

Anders Brask, Jörg P. Kutter and Henrik Bruus

Received 10th March 2005, Accepted 10th May 2005
First published as an Advance Article on the web 31st May 2005
DOI: 10.1039/b503626g

We present the design, fabrication and test of a novel inline frit-based electroosmotic (EO) pump with ion exchange membranes. The pump is more stable than previous types due to a new flow component that ensures a controlled width of the diffusion layer close to the ion exchange membranes. The pump casing is constructed in polymers while the EO active part, the frit, is made in a nanoporous silica. The pressure capability of the pump is $\Delta p_m/\Delta V = 0.15$ bar V^{-1}. The flow rate to current ratio is $Q_m/I = 6$ μL min^{-1} mA^{-1}. This translates to $\Delta p_m = 4.5$ bar and $Q_m = 6$ μL min^{-1} at $\Delta V = 30$ V. The pump has been tested with four different buffer concentrations. In order to investigate day-to-day reproducibility each Q–p pump characteristic has been recorded several times during hour-long operation runs under realistic operating conditions.

1 Introduction

Electroosmotic (EO) pumps are suitable for microfluidic applications because they can be made very compact and deliver high pressures. Moreover, they can produce a pulse-free flow without containing any moving parts. In EO pumps an electrolyte is pumped by applying an electric field to the charged Debye layer. The Debye layer is formed by the ions in the electrolyte due to electric screening of the immobile charges on the walls of the pump.[1] Traditionally, EO pumps are driven by voltages in the kilovolt range,[2–4] but in many applications high voltages are impractical. As a consequence a low-voltage EO pump was presented by Takamura *et al.*[5] and analyzed by Brask *et al.*[6] This low-voltage pump design allows for arbitrary pressure accumulation without increasing the voltage. However, EO pumps based on porous structures have proved to produce very high pressures with simpler geometries.[7–10] A high flow rate variant of the porous EO pump is the so-called frit-based EO pump.[11,12] For a recent review of micropumps see ref. 13.

Some of the inherent problems for continuously operated DC EO pumps are the development of electrolytic gases and long-term stability. The gas development issue is traditionally avoided by separating the electrodes from the electroosmotic pumping with an ion exchange system[2,3,5,7] or by using induced hydraulic pumping.[14] A system that recombines the electrolytic gases has been reported by Yao *et al.*[12]

The work presented here differs from most previous work on EO pumps by emphasizing stability. In particular, we investigate and address some of the stability issues for EO pumps with ion exchange membranes. We focus on two main stability criteria. (1) Temporal analysis of the flow rate and pressure under varying operating conditions. (2) The day-to-day reproducibility, *i.e.*, the importance of proper priming and conditioning.

The paper is organized in the following way. In Sec. 2 the basic equations and concepts for electroosmotic pumping are presented. In Sec.3 we present the final EO pump design as a result of a long development history. The functionality and design of the individual components are described in detail. In particular, the concept of limiting current density is introduced in relation to EO pumps with ion exchange membranes. In Sec. 4 the fabrication of the pump is described. In Sec. 5 we deal with the fluidic setup and the measurement protocol. Finally the results and conclusions are presented in Sec. 6 and Sec. 7, respectively.

2 A model of EO flow in a frit

Our aim is to develop a long-term stable EO pump with high flow rate and pressure capacity. At the same time we want to use a low driving voltage. The solution is to use a structure with a large number of nanochannels. A nanoporous frit fulfills these requirements, see Fig. 1.

To a first approximation the geometry of the porous frit may be modelled as a large number of parallel coupled capillaries with length L and radius a. The cross sectional area and thickness of the frit is denoted A and L, respectively. The porosity is defined as $\psi = v_e/v$ where v_e is the void volume of the frit, *i.e.*, the volume available to an electrolyte solution and $v = AL$ is the total volume.

The surface charge generates a potential distribution within the capillaries. In a cylindrical capillary this can be solved analytically for a symmetric electrolyte by invoking the

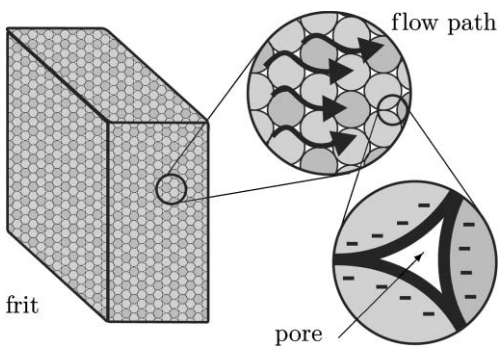

Fig. 1 A rough sketch of a frit. The frit is made of a porous material, in this case silica. When silica comes in contact with an electrolyte it typically forms a negative surface charge. This effect makes the silica frit ideal for electroosmotic pumping.

Debye–Hückel approximation in the Poisson–Boltzmann equation.[15] The governing equations for the theoretical Q–p performance of a frit based EO pump are as follows:

$$Q_{\mathrm{m}} = \alpha_{\mathrm{eo}}\psi\frac{A}{L}\left[1-\frac{2\lambda I_1(a/\lambda_{\mathrm{D}})}{aI_0(a/\lambda_{\mathrm{D}})}\right]\Delta V, \quad (1)$$

$$\Delta p_{\mathrm{m}} = \alpha_{\mathrm{eo}}\frac{8\mu}{a^2}\left[1-\frac{2\lambda I_1(a/\lambda_{\mathrm{D}})}{aI_0(a/\lambda_{\mathrm{D}})}\right]\Delta V, \quad (2)$$

$$\lambda_{\mathrm{D}} = \left(\frac{\varepsilon kT}{e^2\sum_i c_i z_i^2}\right)^{1/2}, \quad (3)$$

$$Q = Q_{\mathrm{m}}\left(1-\frac{\Delta p}{\Delta p_{\mathrm{m}}}\right). \quad (4)$$

Here, α_{eo} is the electroosmotic mobility, μ the dynamic viscosity, ε the dielectric constant of the electrolyte, ΔV the applied voltage, c_i and z_i the concentration and valence of the i-th species, respectively. λ_{D} is the Debye length, Q_{m} the maximum flow rate, and Δp_{m} the maximum backpressure. I_k is the k'th-order modified Bessel function of the first kind. For more details see ref. 9.

The term in the brackets in eqns. (1) and (2) is denoted the correction factor. In the case of $a/\lambda_{\mathrm{D}} \gg 1$ the correction factor equals unity. If the channel radius a and the Debye length λ_{D} become comparable, the flow Q_{m} is reduced due to an effect termed Debye layer overlap, *e.g.*, for $a/\lambda_{\mathrm{D}} = 1$ the correction factor is 0.11. Starting from large values of a/λ_{D} the electroosmotic pressure increases with decreasing a/λ_{D} until $a/\lambda_{\mathrm{D}} \approx 1$ hereafter it does not change considerably.

A nanoporous silica frit is chosen as the pumping media because it gives a high flow rate, $Q_{\mathrm{m}} \propto A$, and a high back-pressure capacity, $p_{\mathrm{m}} \propto a^{-2}$, see eqns. (1) and (2). Furthermore, it is also commercially available and easy to integrate.

3 The design

The frit-based EO pump consists of an assembly of nine layers as shown in Fig. 2. The electrode compartments formed by α and β are separated from the frit compartment ε by anion exchange membranes (AEM) γ, which allow only anions (negative ions) to pass, while bulk fluid and positive ions are retained. The pressure buildup generated by the frit is therefore confined to the inner loop of the pump, δ–ε–δ, which enables free ventilation of electrolytic gases developed in the electrode compartments.

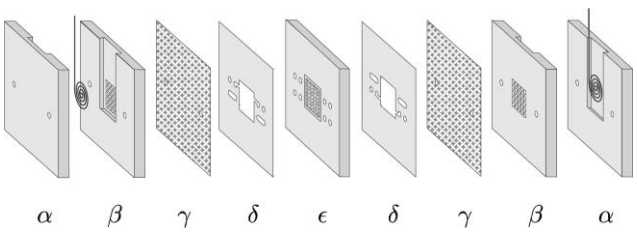

Fig. 2 Schematic view of the functional components in the EO pump: Electrode chamber (α), electrode chamber and membrane support (β), ion exchange membrane (γ), spacer and bypass system (δ), and frit holder and through-holes for the bypass system (ε).

3.1 The frit

Electroosmosis is based on separation of charges where one polarity is mobile in the electrolyte and the other is immobile on the wall. The surface charge density and pore size are very important in relation to the performance. The frit considered here is based on silica (SiO_2), a material that will typically form a negative surface charge. The EO flow direction is hence from the anode to the cathode. The surface charge and hence the EO mobility is highly dependent on pH,[2]

$$\text{Surface at pH} > 3\text{: Si–OH} \rightarrow \text{Si–O}^- + \text{H}_2\text{O},$$

$$\text{Surface at pH} < 3\text{: Si–OH} \rightarrow \text{Si–OH}_2^+.$$

A constant pH level is required for stable operation. In fact, this is a problem in many previously reported EO pumps.[7,16] A more detailed discussion on how to maintain a stable pH follows in the next sections.

3.2 Ion exchange membranes

The pumping stability is governed by the pH and flow conditions in the inner loop, δ–ε–δ in Fig. 2. At the anode the pH will tend to drop because of the generation of hydronium ions (solvated H^+). A low pH environment will effectively remove the surface charge in the frit and thus stop the EO flow. To stabilize the pH level we insert an anion exchange membrane capable of preventing the hydronium ions from entering the inner loop. In this way the pump will continue to work after the buffer in the reservoir has been depleted. The anion exchange membrane only allows negative ions to pass because of the Donnan exclusion principle.[17]

Since most of the hydronium ions will be blocked by the AEM the electric current in the stationary state will be transported mainly by hydroxyl OH^- and sodium Na^+ ions.

The second main function of the ion exchange membranes is that they block bulk flow. The ion exchange membranes are made of a nanoporous polymer with a permanently charged surface. The pores are so small that they act exclusively as ion channels. The pressure driven flow through the membranes is therefore negligible. As a consequence, both reservoirs can be kept at atmospheric pressure allowing for free ventilation of electrolytic gases. Over a period of two hours this system works well but eventually the reservoirs would need to be refilled due to evaporation and electrolytic gas generation.

3.3 Spacer

Let us consider an ion exchange membrane immersed in an electrolyte solution. The ionic concentration within an ion exchange membrane is usually a factor 10^1 to 10^3 higher than in the ambient liquid. The membrane phase therefore conducts electric current much better than the liquid phase, see Fig. 3. Hence, after a while the liquid in the vicinity of the cathode side of the membrane will be depleted of ions. Diffusion of ions from the bulk will contribute to the transport and try to equalize the ion concentration. If, however, the current density exceeds a certain threshold the slow diffusion current cannot bring in new ions fast enough. The consequence is that the ion concentration at the membrane surface is zero. This threshold

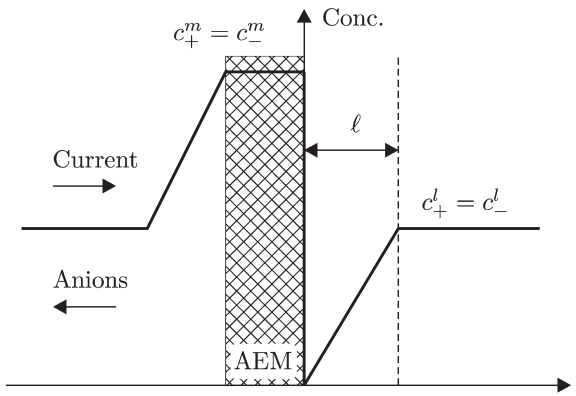

Fig. 3 Schematic figure of the concentration of ions in the vicinity of the anion exchange membrane (AEM). The membrane phase has a much higher concentration of ions $c_{\pm}^{m} \approx 1$ M compared to the bulk solution $c_{\pm}^{l} \approx 10$ mM. Only the anions are mobile in the membrane phase. In the presence of a current this imbalance in concentration and hence conductivity will lower the ionic concentration on the cathode side of the AEM. Convection in the bulk ensures a constant concentration at a distance ℓ from the membrane. In the depicted situation the current equals the limiting current density $i = i_{\mathrm{lim}}$.

is called the limiting current density i_{lim}. An expression for the limiting current density i_{lim} can be derived from an assumption that there exists a diffusion boundary layer of thickness ℓ:

$$i_{\mathrm{lim}} = z_- \left(1 + \frac{z_-}{z_+}\right) F D_- \frac{c_-^{l}}{\ell}. \qquad (5)$$

Here, z_- and z_+ are the charge coefficients of the anion and cation species, respectively, D_- is the diffusion coefficient of the anions, F is the Faraday constant, and c_-^{l} is the concentration of the anions in the liquid phase.

If the current density i is increased beyond i_{lim}, dissociation of water will happen on the surface of the membrane facing the frit. Experimentally this can be observed by a plateau in the current–voltage characteristic.[17] The dissociation of water will increase the hydronium ion concentration in the frit and lower the pH, which in turn affects the stability negatively. Therefore, in order to increase the limiting current the diffusion length ℓ must be decreased. This can be realized by having a very thin spacer between the membrane and the frit. This spacer of width 90 μm is denoted δ in Fig. 2. The spacer layer is designed such that the flow entering the frit has to pass over the membrane at the same time. The induced convection adds to the transport of ions and hence increases the limiting current i_{lim}.

The boundary diffusion layer is associated with a large electrical resistance because of the low ionic concentrations. The consequence is that the electric current I is slightly dependent on the flow condition $Q(\Delta p)$ at a fixed voltage ΔV. A more in-depth computational study of this diffusion–convection problem is, however, beyond the scope of this work.

3.4 Membrane support

The anion exchange membrane is relatively thin, about 140 μm, and must therefore be mechanically supported. The support structure β consists of a 5 by 5 matrix of 1 mm deep through-holes. The array of holes allows the electrolyte in the reservoir to be in contact with the membrane without allowing the membrane to deflect considerably. Keeping the compliance of the pump to a minimum in this way is important in relation to the response time of the pump. A typical response time is 1 min measured from the change in backpressure Δp to the time where the flow rate Q is stabilized again. Together with the back plates α the membrane supports form the reservoirs. Each reservoir contains $v_{\mathrm{res}} = 75$ μL of buffer. Bubbles are expected in the reservoirs due to electrolysis, and they can accumulate in the through-holes of the membrane support mesh. If this happens the current and hence the pumping will decrease. An additional hydrophilic fiber mesh was therefore inserted between the electrode and the membrane support mesh in order to prevent this from happening.

4 Fabrication

All layers have been fabricated from a polymer substrate by laser ablation,[18,19] with a 65 W CO_2 laser from Synrad Inc. (Mukilteo, WA, USA). The α, β and ε layers are made in 1.5–2 mm thick polymethylmethacrylate from Nordisk Plast (Auning, Denmark). The material is chosen because of its ideal properties for laser ablation. The gaskets and spacer layers δ were made in 90 μm thick thermoplastic elastomer from Kraiburg Gummiwerke (Waldkraiburg, Germany).

The layers α and β are bonded together thermally. The rest of the layers are pressed against each other by nuts and bolts; note that the holes for the bolts are not shown in Fig. 2. This construction allows for rapid interchange of components. The alignment is accurate within 300 μm. External tubing was mounted in layers α and β by making two threaded holes. The tubing was then screwed in and fixed with a small amount of epoxy. This fixture was proven to be tight at pressures in excess of 7 bar.

In the experiments described here a pure silica frit from Advanced Glass and Ceramics (Holden, MA, USA) with a nominal pore size of 200 nm and dimensions $5 \times 5 \times 2$ mm^3 was used. The frit was bonded to a holder ε by use of epoxy.

The ion exchange membrane was purchased from Fuma-Tech (Vaihingen an der Enz, Germany). The membrane is quite thin, about 140 μm, which reduces problems with swelling. One complication with this particular membrane is that it must be hydrated at all times. If the membrane is dehydrated it may form tiny stress cracks causing leaks.

All the experiments have been performed with borate buffer only. The concentration of the borate buffer is measured in terms of the molar concentration of $Na_2B_4O_7$. The buffer has a pH = 9.2.

5 Measurements

The focus of the experimental work is the long-term performance of the pump under realistic working conditions. The setup could be operated without simultaneously having to manipulate the pump or the fittings. This is a clear advantage when investigating reproducibility.

5.1 Fluidic setup

Valves and fittings (Upchurch Scientific, Oak Harbor, WA, USA) were mounted on a custom made table with 1/2″ spaced

threaded holes, see Fig. 4. Flow rates Q were measured by collecting liquid in a 25 mL reservoir placed on a balance with 0.1 mg precision (Sartorius CP224S, Goettingen, Germany). The change in mass of the reservoir could then be translated into a flow rate by dividing with the density of the liquid. The reservoir pressure (backpressure) was controlled by a N_2 source. The backpressure $\Delta p = p_2^{\text{sens}} - p_1^{\text{sens}}$ was measured by two 0–10 bar Honeywell pressure sensors (40PC150G1A, Freeport, IL, USA) placed upstream and downstream of the pump, see Fig. 5. Suspended flexible tubing was used to connect the collecting reservoir in order to minimize the transfer of forces from the tubing to the balance. After placing the reservoir on the balance it would take 30 min before the flexible tubing and hence the balance had settled. The preferred tubing material is polyvinylchloride because of its water impermeability. Silicone tubing is not suitable because the water content of the buffer can evaporate and leave large crystals that can block the tubing. In the remainder of the fluidic setup teflon tubing with an inner diameter of 0.5 mm was used giving negligible pressure losses while maintaining a small system volume.

During the measurements six variables were sampled at 1 Hz into a data file using LabView with a 16-bit data acquisition card (National instruments, Austin, TX, USA). The variables are voltage ΔV, current I, upstream pressure p_1^{sens}, downstream pressure p_2^{sens}, mass of reservoir m, and elapsed time t. Before and after the experiments the pH levels in the reservoirs were measured by four color pH indicators.

5.2 Priming of the pump

In order to test the pump in a reproducible manner the pump and external tubing must be free of air bubbles. Bubbles can be removed by flushing the system. In Fig. 6 a flow diagram of the flushing system is shown.

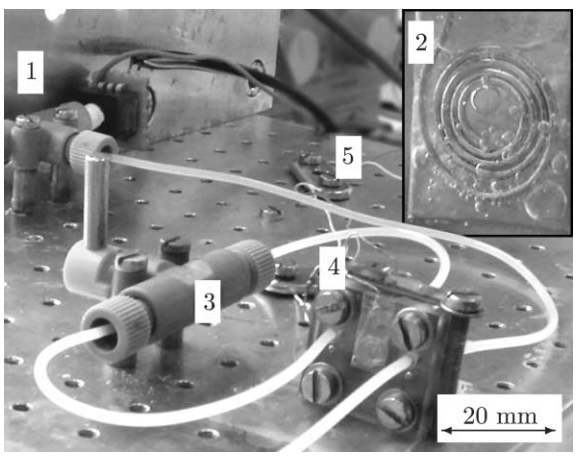

Fig. 4 Picture of the EO pump and the part of the fluidic test setup illustrated in Fig. 5 within the dashed box. (1) Pressure sensor embedded in a tee junction. (2) An inset showing a magnified view of the electrode chamber of the EO pump. A hydrophilic fiber mesh (not visible) has been inserted between the spiral shaped Pt electrode and the membrane support mesh in order to prevent the visible bubbles from blocking the current. (3) External bypass valve. (4) The assembled EO pump measures 20 × 20 × 10 mm^3. (5) The power leads for the pump.

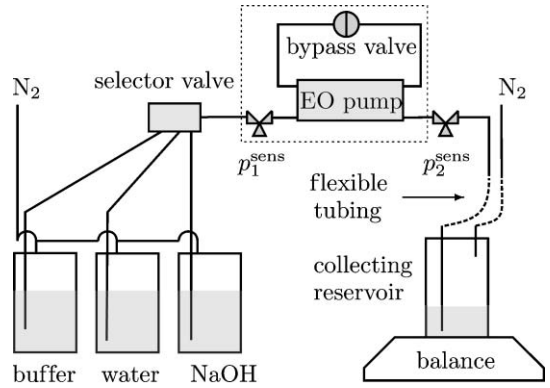

Fig. 5 Schematic diagram of the experimental setup. A selector valve is used for selecting the solution that goes into the EO pump. Pressurized N_2 is used for driving the solutions when priming the pump. During measurements this external pressure is used for setting the backpressure on the pump. Flexible tubing is used for connecting the balance reservoir in order to minimize the forces from the tubing. A vacuum could be applied to the collecting reservoir in order to empty it without disturbing the flexible tubing. The components within the dashed box are depicted in Fig. 4.

A flushing system is required because of the very large hydraulic resistance of the frit, about 200 bar μL^{-1} s. In the flushing mode the flow can bypass the frit which reduces the hydraulic resistance by a factor of 10^3. In the flushing mode it is hence possible to prime the pump and remove bubbles from the system.

Once all bubbles have been removed the conditioning of the frit may begin. The purpose of the conditioning is to ensure that the surface charge, *i.e.*, the EO mobility, is the same within a series of experiments. The conditioning is performed by flushing three different liquids through the frit. First a strong alkaline solution 0.1 M NaOH is used to regenerate the surface charge. Then deionized water is used to remove the alkaline solution and finally the frit is flushed with the buffer, $Na_2B_4O_7$.

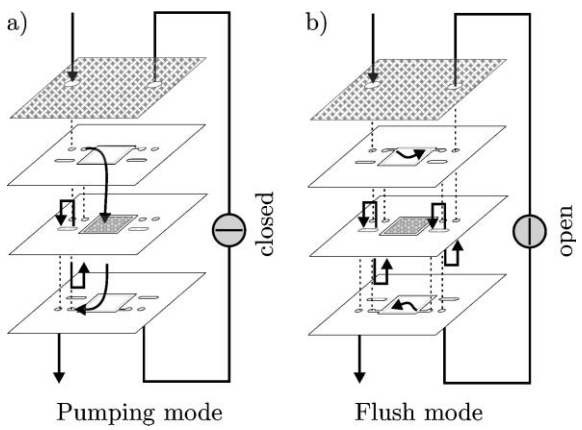

Fig. 6 Flow diagram of the two modes of the flush system. (a) Pumping mode: the external bypass valve is closed. Hence the electrolyte can only pass through the frit. (b) Flushing mode: the external bypass valve is open. In this mode the flow can bypass the frit allowing for fast interchange of fluid within the pump. Note that the flow is directed through the frit holder ε and back. This flow routing eliminates problems with leakage from the inner loop δ–ε–δ to the electrode reservoirs α–β.

The internal volume of the system is 70 μL from the selector valve to the EO pump, see Fig. 5. Hence, an intermediate flush of 400 μL or more is applied with the bypass valve open after a change in the selector valve's position. This is done to make sure that the electrolyte in the tubing has been replaced before the bypass valve is changed into the pumping mode.

The maximum pressure that can be applied safely to the frit compartment is about 2 bar. At that pressure the flow rate is Q = 2 bar/(200 bar μL^{-1} s) = 10 nL s^{-1}. The volume of the frit is approximately $v_e = v \times \psi$ = 15 μL, where v = 5 × 5 × 2 mm^3 and ψ = 0.3. It therefore takes roughly half an hour to flush one void volume v_e of the frit. Optimally, one would like to flush the frit void volume several times. However, in order to save time the frit void volume is only flushed a little more than one time with each of the three solutions. Once the flushing volume exceeds the frit void volume no further dependence of flushing volumes was observed in the experiments. The exact flushing volumes from each experiment are listed in Table 1.

5.3 Measurement protocol

A protocol for the execution of the measurement was established in order to make experiments more comparable. After priming, the pump would be operated for 1 h with no backpressure, Δp = 0. Then about ten measurements at different backpressures would be made, see Fig. 7. Each measurement lasts 6 min and is divided into two parts. During the first 3 min the backpressure is set and the system allowed to adjust accordingly. The next 3 min are used for the actual measurement. The time span of a measurement is indicated in Fig. 7 with vertical dashed (start) and solid (stop) lines. The thick solid horizontal lines indicate the calculated average in each measurement.

The backpressure is set by increasing or decreasing the amount of compressed air in the collecting reservoir. Once the desired pressure level has been reached the air valve is closed. In some of the initial measurements the backpressure was not entirely constant over the period of a measurement due to air leaks in the collecting reservoir. This constitutes a source of error in the flow rate measurements because the loss of air pressure is associated with the mass of the reservoir. To correct for this error the mass of the compressed air is included in the flow rate calculations. This is also why the calculated average sometimes is slightly above the flow rate markings.

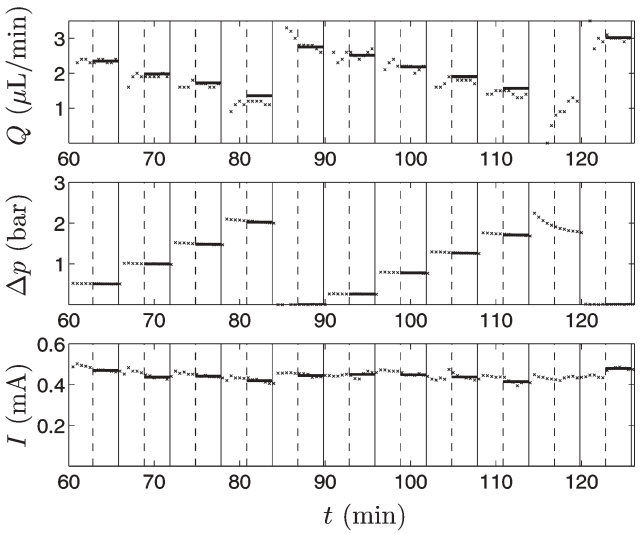

Fig. 7 Flow rate Q, backpressure Δp and current I as function of time for experiment No. 3 in Table 1. The backpressure is increased in four steps. Then the pressure is released to check that the pump recovers its baseline. This procedure is then repeated, now with five steps in Δp. In each measurement there is a black horizontal line indicating the value transferred to the Q–p diagram. If a measurement for some reason is invalid there is no line. Flow rate measurements are based on a sliding average of width 1 min.

The standard protocol was that the backpressure was gradually increased. Once the backpressure reached the maximum testing pressure of around 3 bar the pressure was released in order to check that the pump recovered its free flow rate Q_m. This procedure was then repeated one more time. In each measurement there is a black horizontal line indicating the value transferred to the Q–p diagram. If a measurement for some reason is invalid there is no line.

The minimum flow rate is of the order Q = 1 μL min^{-1}. This corresponds to collecting 1 mg min^{-1} of liquid which should be compared with the minimum measurable mass of 0.1 mg. A flow rate measurement should be based on collecting at least

Table 1 An overview of the Q–p characteristics. The data is divided by concentration into four series with c = 1, 5, 20, 100 mM. The number (No.) is used for reference in this paper. The pH values in the (A)node and (C)athode chamber are measured after approximately 2 h of pumping. The preflush sequence is 1 M NaOH/deionized water/buffer. The applied voltage is ΔV = 30 V in all of the experiments

Conc./mM	No.	(p_m/Q_m)/bar μL^{-1} s	R_{hyd}/bar μL^{-1} s	(p_m/I)/bar mA^{-1}	(Q_m/I)/μL min^{-1} mA^{-1}	pH A/C	preflush/μL
1	11	59	138	4.9	4.9	3/11	47/85/62
1	12	74	139	6.6	5.3	3/11	42/63/92
1	13	92	134	7.9	5.1	—	25/34/85
1	14	53	135	5.3	5.9	—	32/32/33
5	1	108	192	9.6	5.3	—	18/18/22
5	2	123	195	11.6	5.7	6/12	21/22/47
5	3	102	186	10.2	6.0	—	22/36/24
20	7	67	157	7.2	6.5	3/13	28/20/29
20	8	68	152	5.9	5.3	2/13	34/52/40
20	9	78	151	8.3	6.4	2/13	17/27/41
20	10	75	144	8.0	6.4	5/13	36/54/90
100	4	46	—	1.9	2.5	—	48/-/193
100	5	53	—	1.7	1.9	5/13	44/-/46
100	6	61	153	1.8	1.8	—	33/-/46

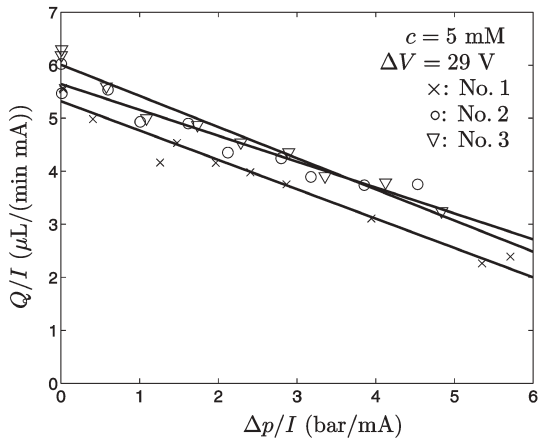

Fig. 8 Experimental data of flow rate Q *vs.* backpressure Δp. The current in the experiments was approximately $I = 0.5$ mA, see Fig. 7. The performance was therefore $Q_m = 3$ μL min^{-1} and an extrapolated maximum backpressure $\Delta p_m = 5$ bar. Experimental parameters can be found in Table 1.

ten times the minimum measurable mass. In this case this requirement limits the temporal resolution of the flow rate measurements to 1 min.

6 Results

Because it takes about six hours to make one Q–p characteristic each characteristic was made on separate days. The pump remained unchanged in all of the experiments. In Table 1 the complete list of experiments is shown. The experiments are labelled chronologically from 1 to 14. The bubbles in the reservoirs can induce some fluctuations in the current and hereby also in the flow rate Q. In the following this effect is removed from the data by monitoring the flow rate and the pressure relative to the current instead of the voltage.

6.1 Pressure characteristics

In Fig. 8 three pump characteristics are shown. Each characteristic consists of about ten sets of corresponding flow rates and backpressures as described in Sec. 5. A linear fit is added to each Q–p characteristic to guide the eye. The three different realizations do collapse onto each other reasonably well. Experiment No. 1 falls slightly under No. 2 and No. 3 but has a similar slope. The average backpressure and flow rate are $\Delta p_m/I = 10.5$ bar mA^{-1} and $Q_m/I = 5.7$ μL min^{-1} mA^{-1}, respectively. The variations are less than 10% for the backpressures and 6% for the flow rates. The maximum available backpressure is an extrapolated value based on the Q–p measurements. The uncertainty on Δp_m is therefore larger than on Q_m.

The four series of Q–p characteristics with different buffer concentrations are shown in Fig. 9. The variation within the same series, *i.e.*, same concentration, gives us information about the reproducibility. Overall, the $c = 5$ mM case appears to give the best results regarding Q_m/I, $\Delta p_m/I$ and reproducibility.

6.2 Efficiency and diffusion layer

The efficiency η of a pump is defined as the hydraulic power $Q\Delta p$ divided by the electrical power consumption $I\Delta V$.

$$\eta = \frac{Q\Delta p}{I\Delta V}. \tag{6}$$

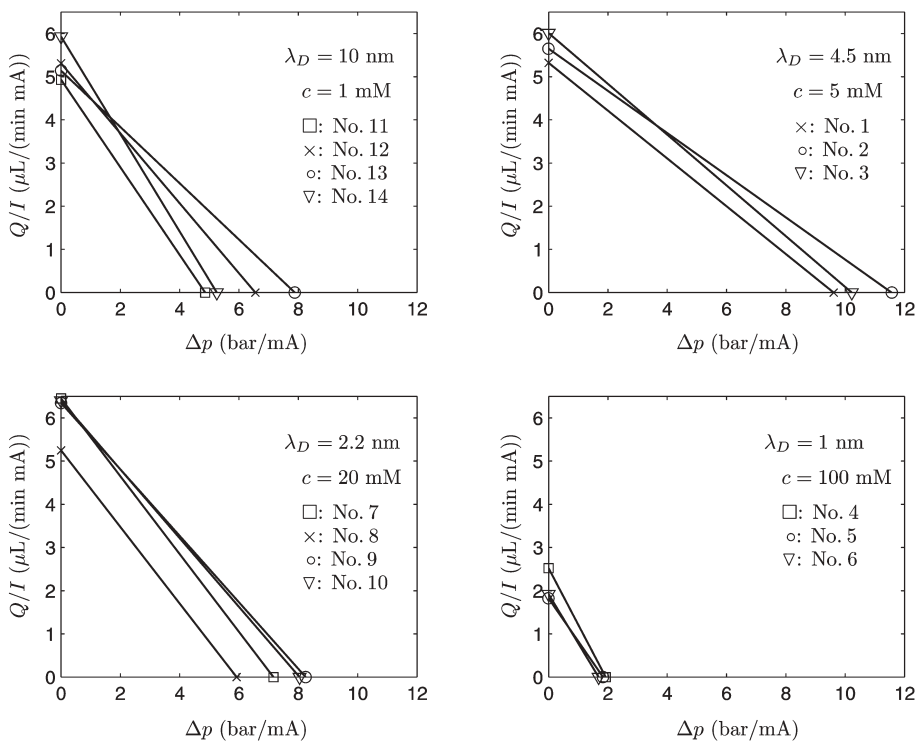

Fig. 9 Q–p characteristics from all 14 experiments displayed for comparison. Note that the axis dimensions in the four figures are the same. The lines are extrapolated best fits from the experimental data.

By inserting eqn. (4) in eqn. (6) and differentiating, it is found that the maximum hydraulic power is obtained with $\Delta p = 0.5\ \Delta p_m$ and $Q = 0.5 Q_m$. The maximum efficiency is hence $\eta_m = 0.25 Q_m \Delta p_m / (I \Delta V)$.

In all experiments the current is initially very high and then decreases rapidly on a time scale of $t = 5$ s, Fig. 10. The time scale is believed to be controlled by the diffusion layer width between the AEM and the frit. A simple estimate yields, $L = \sqrt{Dt} = 105\ \mu$m which compares well with the thickness of the 90 μm spacer layer. An additional investigation showed that this time scale is independent on the type of frit used.

The large drop in the current indicates that the main potential drop lies across the diffusion layer adjacent to the ion exchange membranes. As a consequence the efficiency of the pump is low, $\eta = 0.04\%$ for $c = 5$ mM, compared to other reported EO pump efficiencies: 0.05–0.3% in ref. 12, 1–3% in ref. 7, and 5.6% in ref. 8. The conclusion is that the anion exchange membranes contribute to the stability but consume a considerable amount of energy. In this work stability was given a higher priority than efficiency. In our opinion stability issues have not been given proper attention in the literature. However, these issues are in fact very important from a practical point of view.

6.3 Flow rate and electric current

The flow rate Q_m is proportional to the electric current I in the free flow setup, see Fig. 11. This is not a surprising result, in fact the current is a much more direct handle on the flow rate than the voltage. Bubbles and polarization effects make it more difficult to monitor the effective voltage than the current. In applications it would therefore be recommended to regulate the pump by current instead of by voltage.

The electrical resistance of the diffusion layer is dependent on the flow rate Q because of the spacer layer, see Sec. 3.3. As a consequence the current I is also dependent on the flow rate $Q(\Delta p)$ for a fixed voltage ΔV, see Fig. 12. The membrane is not completely fixed between the membrane support and the spacer. The membrane can buckle due to swelling and the position can be shifted due to pressure changes. Changes in the position of the membrane can change the flow pattern over the membrane and hereby change the electrical resistance of the diffusion layer. It was observed that the I–Q curves for fixed voltage ΔV varied considerably, Fig. 12. A better control of the gap between the membrane and the frit is required in order to improve reproducibility.

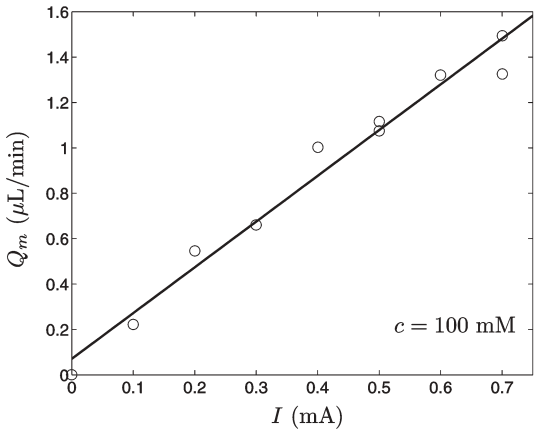

Fig. 11 Experimental data of the free flow rate Q_m *vs.* current I. The current is held fixed at $I = 0.1$, 0.2, 0.3, 0.4, 0.5, 0.6 0.7 mA, respectively by regulating the voltage. The flow rate is proportional with the current as expected. The slope $Q_m/I = 2.1$ μL min^{-1} mA^{-1} is similar to what is observed in experiments No. 4–6.

6.4 Limiting current

The limiting current density may be calculated on basis of eqn. (5). Using the values $\ell = 90\ \mu$m, $D = 2 \times 10^{-9}$ m^2 s^{-1}, $z_- = z_+ = 1$, $c_-^l = 2c$ we obtain $i_{lim} = 8.6, 43, 172, 858$ A m^{-2} for $c = 1$, 5, 20, 100 mM, respectively. By multiplying the current density with the area of the membrane $A = 5 \times 5$ mm^2 we obtain $I_{lim} = 0.21$, 1.1, 4.3, 21 mA. Typical currents in the experiments were $I = 0.2$, 0.5, 0.8, 2 mA for $c = 1$, 5, 20, 100 mM, respectively. Thus, in all cases the EO pump was operated below the limiting current density. If, however, the electrolyte within the pump is close to being stagnant the diffusion layer may extend into the frit and thereby lower the limiting current.

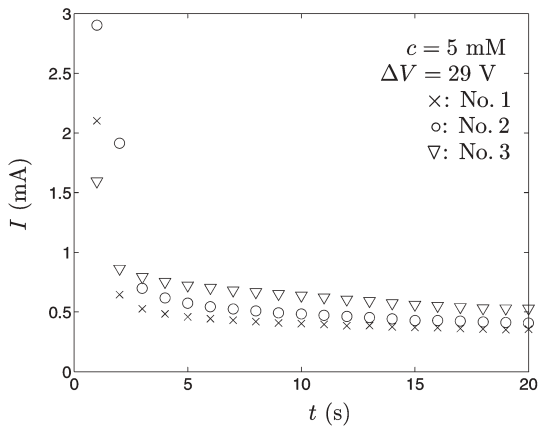

Fig. 10 Experimental data of current I *vs.* time t. The pump is turned on at $t = 0$ s. The current decreases between 50–80% over the first 20 s of operation. Experimental parameters can be found in Table 1.

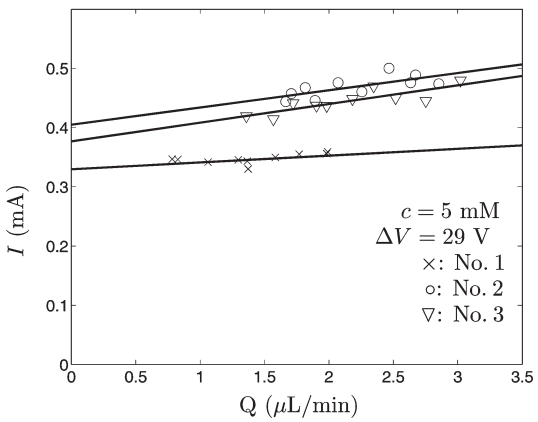

Fig. 12 Experimental data of the current I *vs.* flow rate Q. The flow rate Q is exclusively regulated by the backpressure Δp. Experimental parameters can be found in Table 1.

6.5 Buffer depletion

Due to electrode reactions the pH value in the anode and cathode reservoir will tend to decrease and increase, respectively. Initially, the buffer ensures a constant pH = 9.2, but after a while the finite reservoir volume v_{res} and electrode reactions cause the buffer to deplete. A rough estimate on the depletion time t_{dep} is given as

$$t_{dep} = \frac{c v_{res} F}{I}. \quad (7)$$

Here, F is the Faradaic constant, v_{res} = 75 μL the reservoir volume, I = 0.5 mA the electric current and c = 5 mM the buffer concentration. With these values the depletion time is t_{dep} = 72 s. The pump is operated over a period of two hours. Hence, we conclude that the initial amount of ions in the reservoir is very small compared to the total molar charge exchange over time. The pH values in the electrode reservoirs are measured after the experiment, see Table 1. Typical values are pH = 3 and pH = 13 in the anode and cathode reservoir, respectively. The conclusion is that the pump works fine with a depleted buffer due to the anion exchange membranes. This stands in contrast to capillary based EO pumps that require large reservoirs and small currents in order to obtain a stable pH and a reasonable lifespan.

6.6 Estimated pore size

To be able to choose a proper buffer concentration, it is important to obtain a good estimate on the pore size of the frit. Three different measurement techniques were applied. Common for the techniques is that they only give an average pore size.

The first method is based on measuring the hydraulic resistance by collecting corresponding values of flow rate and pressure drop, and then use the parallel-capillary model of Sec. 2.

The second method is based on the values of Q_m and Δp_m obtained by operating the pump. If eqns. (1) and (2) are rearranged we obtain

$$a = \sqrt{\frac{8 Q_m L \mu}{\Delta p_m \psi A}}. \quad (8)$$

The third method is to use a scanning electron microscope (SEM) to visualize the surface of the frit. The frit is covered by a 10 nm layer of gold. Unfortunately, the pores are of comparable size, which could be the reason why the image, see Fig. 13, is not very well resolved. However, it is clear that the surface pores are not 200 nm in diameter.

The results from the three different methods are summarized in Table 2. The pore sizes are not as uniform as expected. The hydraulic resistance method probably underestimates the pore size due to electroviscous effects. For a more detailed discussion see ref. 20. The most accurate method to estimate the pore size seems to be based on the $\Delta p_m/Q_m$ ratio.

A complication to the pore size discussion is that the hydraulic resistance R_{hyd} appears to be decreasing over time. If we look at Table 1 we see that R_{hyd} decreases by roughly 30% after 14 experiments. This could be due to structural damage to the frit caused by the treatment with sodium hydroxide before each experiment.

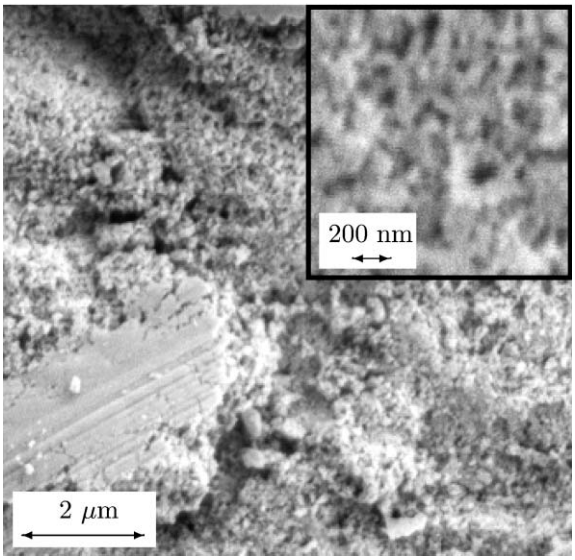

Fig. 13 SEM picture of the silicate frit with 200 nm nominal pore size. The dark areas are the pores. Marks from tooling can be seen in the lower left corner. A magnification shows that the pores appear to be considerably smaller than the nominal pore size of 200 nm. A typical opening is estimated to be 40 nm.

7 Conclusion

A stable stand-alone EO micropump has been developed and successfully tested. The design is highly versatile and can be modified to meet most flow requirements in microfluidic applications. Inherent disadvantages of continuously operated DC electroosmotic pumps are the dependence on the electrolyte and development of electrolytic gases.

The pump has been tested with concentrations of borate buffer (pH = 9.2) in the range c = 1–100 mM. The optimal concentrations were 5 and 20 mM. The 20 mM buffer gave the highest flow rate and backpressure per volt, while the 5 mM buffer gave the highest efficiency η = 0.04%.

The pump has been tested at realistic operating conditions over several weeks and the day-to-day reproducibility is within 6% on the flow rates Q_m for c = 5 mM. Even better reproducibility has been reported for capillary based EO pumps.[2] One of the reasons for this is that it is more difficult to condition the surface of a nanoporous frit. The pump performance does not degrade over the time of the measurement. So the variation in the flow rate Q_m must come from the flushing sequence that is supposed to condition the frit and membranes the same way each time. A more uniform ensemble of nanochannels would be advantageous as well.

The presented inline EO pump is simple and inexpensive in its construction and delivers a precise and stable flow. It is robust against particles and bubbles and is capable of

Table 2 Average diameter of the pores in the frit measured using different methods

Method	Diameter
Hydraulic resistance	24 ± 2 nm
$\Delta p_m/Q_m$	34 ± 8 nm
SEM pictures	40 ± 20 nm

delivering $Q_m = 6\ \mu L\ min^{-1}$ and $\Delta p_m = 4.5$ bar at a low voltage $\Delta V = 30$ V. The buffer in the electrode chambers is depleted after a few minutes. However, the anion exchange membranes allow the EO pump to work even with a depleted buffer. In the scope of this work the tests have been limited to two hours. If the pump is operated for more than two hours the reservoirs need a refill because of evaporation and generation of electrolytic gases. A more enclosed reservoir design would extend the operation time but for true continuous DC operation the electrolytic gases must be recombined. A system capable of recombining the gases in order to avoid this problem has been reported in ref. 12.

Acknowledgements

We would like to acknowledge Torben Jacobsen for helpful discussions on electrochemistry and Maria Dimaki for help with the SEM images. This work is partly supported by the Danish Technical Research Council, μTAS Frame Program Grant No. 26-00-0220.

Anders Brask, Jörg P. Kutter and Henrik Bruus
MIC—Department of Micro and Nanotechnology, DTU Bldg. 345 east, Technical University of Denmark, DK-2800, Kgs. Lyngby, Denmark

References

1 R. J. Hunter, *Zeta Potential in Colloidal Science: Principles and Applications*, Academic Press, London, 1981.
2 P. K. Dasgupta and S. Liu, *Anal. Chem.*, 1994, **66**, 1792.
3 W. E. Morf, O. T. Guenat and N. F. d Rooij, *Sens. Actuators B*, 2001, **72**, 266.
4 C. H. Chen and J. G. Santiago, *J. Microelectromech. Syst*, 2002, **11**, 672.
5 Y. Takamura, H. Onoda, H. Inokuchi, S. Adachi, A. Oki and Y. Horiike, *Electrophoresis*, 2003, **24**, 185.
6 A. Brask, G. Goranović and H. Bruus, *Sens. Actuators B*, 2003, **92**, 127.
7 B. P. Mosier, R. W. Crocker, J. L. Rognlien and K. D. Patel, *Am. Soc. Mech. Eng., FED*, 2003, **259**, 511.
8 D. S. Reichmuth, G. S. Chirica and B. J. Kirby, *Sens. Actuators B*, 2003, **92**, 37.
9 S. Zeng, C. H. Chen, J. C. Mikkelsen and J. G. Santiago, *Sens. Actuators B*, 2001, **79**, 107.
10 W. Gan, L. Yang, Y.-Z. He, R.-H. Zeng, M. L. Cervera and M. Guardia, *Talanta*, 2000, **51**, 667.
11 S. Yao and J. G. Santiago, *J. Colloid Interface Sci.*, 2003, **268**, 133–142.
12 S. Yao, D. E. Hertzog, S. Zeng, J. C. Mikkelsen and J. G. Santiago, *J. Colloid Interface Sci.*, 2003, **268**, 143–153.
13 D. J. Laser and J. G. Santiago, *J. Micromech. Microeng.*, 2004, **14**, R35–R64.
14 C. T. Culbertson, R. S. Ramsey and J. M. Ramsey, *Anal. Chem.*, 2000, **72**, 2285.
15 C. L. Rice and R. Whitehead, *J. Phys. Chem.*, 1965, **69**, 4017.
16 S. Yao, D. Huber, J. C. Mikkelsen and J. G. Santiago, *Proc. IMECE USA*, 2001, **3**, 639.
17 M. Mulder, *Basic Principles of Membrane Technology*, Kluwer Academic Publishers, Dordrecht, 2nd edn., 1996.
18 H. Klank, J. P. Kutter and O. Geschke, *Lab Chip*, 2002, **2**, 242.
19 M. F. Jensen, M. Noerholm, L. H. Christensen and O. Geschke, *Lab Chip*, 2003, **3**, 302.
20 P. Vainshtein and C. Gutfinger, *J. Micromech. Microeng.*, 2002, **12**, 252.

